Available online at www.sciencedirect.com
SCIENCE DIRECT
Surface Science 600 (2006) 1924–1935
SURFACE SCIENCE
www.elsevier.com/locate/susc

The local adsorption geometry and electronic structure of alanine on Cu{1 1 0}

G. Jones [a], L.B. Jones [b,c], F. Thibault-Starzyk [a,d], E.A. Seddon [b], R. Raval [c], S.J. Jenkins [a], G. Held [a,*]

[a] University of Cambridge, Department of Chemistry, Lensfield Road, Cambridge CB2 1EW, UK
[b] CCLRC Daresbury Laboratory, Warrington, UK
[c] Surface Science Research Centre and Department of Chemistry, University of Liverpool, UK
[d] Laboratoire Catalyse & Spectrochimie, CNRS ENSICAEN, Université de Caen, France

Received 7 December 2005; accepted for publication 15 February 2006
Available online 20 March 2006

Abstract

The adsorption of alanine on Cu{1 1 0} was studied by a combination of near edge X-ray absorption fine structure (NEXAFS) spectroscopy, X-ray photoelectron spectroscopy (XPS) and density functional theory (DFT). Large chemical shifts in the C 1s, N 1s, and O 1s XP spectra were found between the alanine multilayer and the chemisorbed $\begin{pmatrix} 2 & -2 \\ 5 & 3 \end{pmatrix}$ and pseudo-(3×2) alaninate layers. From C, N, and O K-shell NEXAFS spectra the tilt angles of the carboxylate group (≈26° in plane with respect to $[1\,\bar{1}\,0]$ and ≈45° out of plane) and the C–N bond angle with respect to $[1\,\bar{1}\,0]$ could be determined for the pseudo-(3×2) overlayer. Using this information three adsorption geometries could be eliminated from five $p(3\times 2)$ structures which lead to almost identical heats of adsorption in the DFT calculations between 1.40 and 1.47 eV/molecule. Due to the small energy difference between the remaining two structures it is not unlikely that these coexist on the surface at room temperature.

Keywords: Alanine; Biological molecules (amino acids); Copper; Near edge X-ray adsorption fine structure (NEXAFS); X-ray photoelectron spectroscopy (XPS); Density functional calculations (DFT); Chemisorption; Surface structure

1. Introduction

Metal–organic interfaces exhibit a great variety of unusual surface phenomena. They depend largely on the coverage and thermodynamic conditions, but also on the chemical states, molecular orientations and intermolecular bonding interactions at the surface [1–3]. In many of these systems, intermolecular forces govern the formation of superstructures, which depend on the balance of molecule–substrate and molecule–molecule interactions [4]. Among the best studied metal–organic surface systems are thin layers of the smallest chiral amino acid, alanine (CH_3–$CH(NH_2)$–COOH), on Cu{1 1 0}. A variety of experimental surface science techniques, such as reflection absorption infrared spectroscopy (RAIRS) [5,6], scanning tunneling microscopy (STM), low-energy electron diffraction (LEED) [7,6], X-ray photoelectron spectroscopy (XPS) [8,6] and photoelectron diffraction (PhD) [9], alongside density functional theory (DFT) ab initio calculations [10] have been used to study the adsorption complex and the long-range arrangement of the molecules on the surface. Of particular interest is the fact that alanine forms chiral superstructure lattices which can exist in two distinguishable and non-superimposable mirror forms (see [1,3,6] and references therein). This system provides a model for both the behaviour of protein-based biomaterials and for heterogeneous asymmetric catalytic systems, where chiral

* Corresponding author. Tel.: +44 1223 336449; fax: +44 1223 762829.
E-mail address: gh10009@cam.ac.uk (G. Held).

0039-6028/$ - see front matter © 2006 Elsevier B.V. All rights reserved.
doi:10.1016/j.susc.2006.02.033

molecules act as chiral modifiers stereo-directing reaction pathways. It has been shown that in the temperature range 300–470 K alanine bonds strongly to the Cu{1 1 0} surface in its deprotonated alaninate form with the integrity of the chiral centre preserved.

The alaninate/Cu{1 1 0} system displays a variety of chiral and achiral surface superstructures, which are discussed in detail in Ref. [6]. In this article we concentrate mainly on the local adsorption structure within the '$p(3\times2)$' enantiopure adsorbate layer. The structure of this most stable alaninate layer, which is formed after annealing to 450 K, has received considerable interest recently. A closer investigation of the LEED pattern (e.g. Fig. 12 in [6]) reveals diffraction spots that are somewhat displaced from the positions expected for a true $p(3\times2)$ structure and that some spots are missing, which has been attributed to an effective glide plane in this structure (a true glide plane symmetry cannot exist in an enantiopure layer). Alternatively, both observations can be explained in terms of a domain structure with larger long-range periodicity and a *local* $p(3\times2)$ arrangement of molecules. This leads to significant intensities only for those spots in the vicinity of a $p(3\times2)$ spot and at the same time to the extinction of the missing spots due to anti-phase domain boundaries without the need of invoking a glide plane. Details of the long-range arrangement of molecules within this structure are the subject of a current study. For the discussion of the local adsorption geometry it is sufficient to assume a simple $p(3\times2)$ overlayer periodicity. In the following, we will refer to this phase as 'pseudo (3×2)' overlayer.

There is general agreement that the alaninate molecules in this phase are in a μ_3 adsorption geometry forming bonds to the Cu surface through their two oxygen atoms and the nitrogen atom which leads to an asymmetric triangular 'footprint' on the surface [6]. A theoretical study by Rankin and Sholl [10] using DFT found optimum structures with footprints very similar to that of glycine (H–CH(NH_2)–COOH) and very little energy difference between racemic and enantiopure structures. Both oxygen atoms and the nitrogen atom were found to be close to atop sites above surface copper atoms. In an independent experimental study, Sayago et al. [9] using PhD were able to determine the positions of the O and N atoms with respect to the Cu atoms, verifying the theoretical predictions of [10]. The positions of these atoms are essentially the same as for glycine on Cu{1 1 0} [11,12]. The backbone carbon atoms, however, could not be located experimentally so far. Their positions, in particular the position of the methyl group, are crucial in understanding the lateral interaction between adjacent molecules, such as van-der-Waals and hydrogen bonding.

Spectroscopies of molecular orbitals, such as angle resolved UV photoelectron spectroscopy (ARUPS) [13,14] or near edge X-ray absorption fine structure (NEXAFS) spectroscopy [15,16], in connection with dipole selection rules have proved to be a powerful alternative approach to crystallographic methods for retrieving information about the orientation of molecules. NEXAFS in particular allows the determination of the orientation of individual moieties within an adsorbed molecule separately, this is because the excitation is confined by the overlap of the final and initial state wavefunctions, the latter of which is usually a localised core level. This technique has been successfully applied by Hasselström et al. [17–19] to determine key geometric and electronic parameters related to the adsorption of glycine and related carboxylic acids on Cu{1 1 0}.

Here we present a combined NEXAFS, DFT and XPS study of alanine adsorbed on Cu{1 1 0}. This combination of techniques provides important additional information about the adsorption geometry, in particular the carbon-backbone of alanine, and the electronic structure of the adsorption complex.

2. DFT calculations

The theoretical section of this article deals with the analysis of possible adsorption geometries and the electronic structure of a representative conformation of alaninate on Cu{1 1 0}.

2.1. Details of the total energy calculations

Density functional theory (DFT) [20] was applied using the computer code CASTEP [21]. Electron–ion interactions were accounted for through ultrasoft pseudopotentials of the Vanderbilt type [22], with exchange and correlation being included at the level of the Perdew–Wang generalised gradient approximation [23] (GGA-PW91). A plane wave basis set expanded to an energy cut-off of 340 eV was used to describe the electronic wavefunctions. Integration over the Brillouin zone was achieved by sampling the Γ-point for the isolated molecule calculations, by summation over a $7\times7\times7$ Monkhorst–Pack mesh [24] for the determination of the bulk Cu lattice constant ($a = 3.606$ Å), and a $3\times3\times1$ mesh for the (3×2) surface calculations. In order to determine heats of adsorption, $p(3\times2)$ unit cells with eight layers of Cu atoms and a vacuum layer equivalent to eight Cu layers deep were employed. Initial trial structures were calculated from four and six layer slabs with good convergence being achieved by eight layers.

2.2. Conformation and initial structures for geometry minimisation

The large body of published experimental [5,17,11,25,1,26] and theoretical work [19,12,10] on the adsorption of glycine and alanine on Cu{1 1 0} all point towards an adsorption geometry where the O atoms of the carboxylate group and the N of the amine group are approximately atop Cu atoms. The earlier theoretical studies show stable geometries in so-called 'heterochiral' and 'homochiral' arrangements with the molecule bridging across two-ridges and each bonding adsorbate atom occupying its own Cu atom.

On Cu{1 1 0} the triangle of the three-point binding footprint is chiral because it is confined to two dimensions, unable to flip around [27,6]. Barlow and Raval [1] have discussed the classification of chiral and achiral species interacting with a surface. Different levels at which chirality can be observed have been described: point (molecular), local and global. The (3×2) phases of alanine and glycine on Cu{1 1 0} exhibit local chirality but no long-range global chirality. The literature describes these overlayers as being locally either 'heterochiral' or 'homochiral'

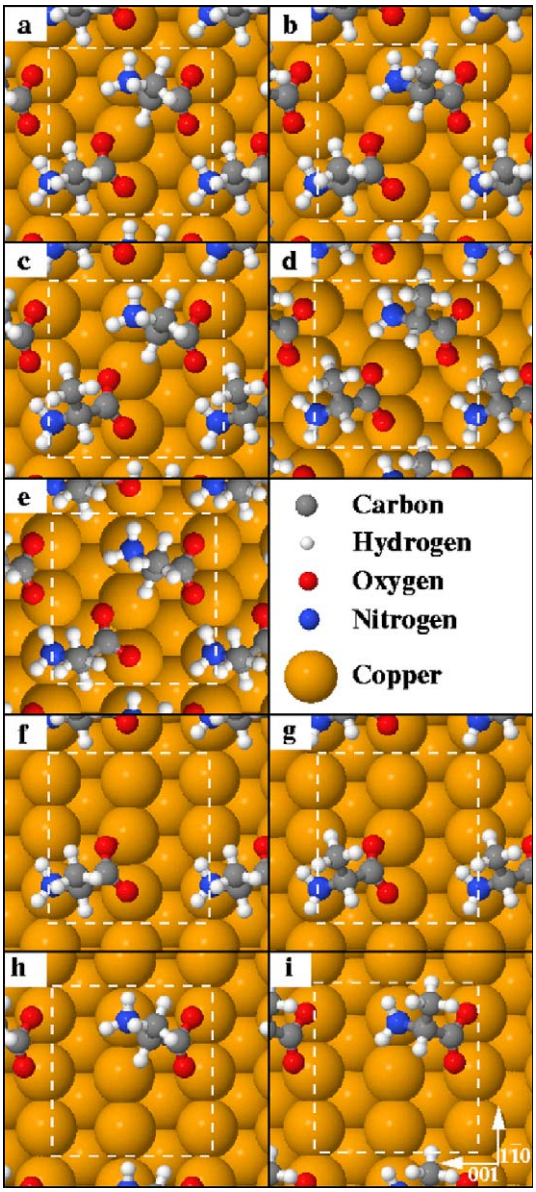

Fig. 1. (a)–(e) Top view of the five enantiopure *R*-alanine $p(3\times2)$ overlayer geometries on Cu{1 1 0} ($\frac{1}{3}$ ML) that led to similar calculated heats of adsorption. Each structure represents a local conformational change primarily noticeable in the backbone orientation of the molecule: (a), (e) kinked/kinked, (b) kinked/linear, (c) linear/kinked, (d) linear/linear. (f)–(i) monomer geometries ($\frac{1}{6}$ ML with a $p(3\times2)$ overlayer periodicity): (f), (h) kinked, different footprints; (g), (i) linear, different footprints. The unit cells are shown as dashed white lines. See text for further details.

[11,25,1,19,26,12,10]. Recently, this description has been further refined in order to discriminate between the intrinsic chirality of the adsorbate ('molecular chirality') and the chirality of the adsorption site ('footprint chirality') [6]. A detailed consideration of the possible binding geometries leads to the realisation that, even for glycine in a $p(3\times2)$ unit cell, the range of molecular orientations is far greater than the two motifs proposed so far. This needs to be accounted for when discussing the precise nature of adsorbed glycine and alanine. Early in this study, we identified two overriding structures for the molecules in question that can be generalised as being kinked or linear. The kinked structure for glycine has the C–H bonds at approximately 25° and 80° to the surface normal, whereas the linear structure has both C–H bonds at an angle from the surface normal close to half the tetrahedral angle, approximately 54°. Similar observations hold for alanine although one C–H bond is, of course, replaced with a C–CH_3 bond. Both 'kinked' and 'linear' molecules can have two different footprints, as shown in Fig. 1(f, h) and (g, i), respectively, for alanine monomers on Cu{1 1 0}.

When filling the binding sites for the proposed (3×2) phase on Cu{1 1 0} with the same enantiomer, there is only one geometry possible that involves only 'kinked' molecules, labelled (a), one with only 'linear' molecules, labelled (d), and two that involve one 'kinked' and one 'linear' molecule each, labelled (b) and (c). In all geometries the two molecules in the unit cell have bonds to three surface copper atoms with opposite footprint chiralities, otherwise the unit cell could not accommodate them. In Fig. 1(a)–(d) these adsorbate geometries are depicted; their key structural parameters are listed in Table 1. Fig. 1 shows optimised geometries after starting with pure 'linear' and 'kinked' molecular backbones. In addition, a fifth energy minimum was found for the geometry depicted in Fig. 1(e), which is similar to (a) with the exception of a substantial buckling of the O atoms in one of the two molecules. In this sense (e) is also similar to the 'homochiral' structure found by comparable calculations of Rankin and Sholl [10], whose work whilst employing a different code essentially uses the same plane wave approach and exchange-correlation functional. From the geometric parameters shown in Table 1 it can be seen that (d) most closely resembles the 'heterochiral' structure of Rankin and Sholl [10]. All five geometries are different from each other, but do lead to very similar adsorption energies, between 1.40 and 1.47 eV per molecule, which is within the error bar of DFT. In this work we only show figures for *R*-alanine; the arguments discussed, however, equally apply for the *S*-enantiomer.

2.3. Electronic structure

For a comparison with the NEXAFS data the density of states (DOS) of the unoccupied electronic states above the Fermi level was calculated. Fig. 2 shows the total DOS of the four structural conformations (a)–(d) (cf. Fig. 1) for

Table 1
Structural parameters for the pseudo-(3 × 2) alanine/Cu{1 1 0} layer as determined by different methods

	ΔH_{ads} (eV molecule^{-1})	d(N–Cu) $\|\|[1\bar{1}0]$ (Å)	d(N–Cu) $\|\|[0\,0\,1]$ (Å)	$\beta_{N\text{-}C}$ $w/r[1\bar{1}0]$ (°)	d(O–Cu) $\|\|[1\bar{1}0]$ (Å)	d(O–Cu) $\|\|[001]$ (Å)	$\alpha_{O\text{–}C\text{–}O}$ out-of-plane (°)	$\alpha_{O\text{–}O}$ $w/r[1\bar{1}0]$ (°)	$I_{[0\,0\,1]}/I_{[1\bar{1}0]}$ [a]
NEXAFS[b]				90			45	26	3.6/5.2
PHD [9]		0.20	0.24		0.12/0.50	1.06/0.46		18[c]	9.5
DFT[b]									
(a) $\frac{1}{3}$ ML	1.45	0.24, 0.14	0.09, 0.08	87, 52	0.12/0.44; 0.31/0.02	0.12/1.00; 0.81/0.64	36, 34	27, 5	8.6
(b) $\frac{1}{3}$ ML	1.40	0.22, 0.29	0.06, 0.11	85, 77	0.04/0.45; 0.35/0.00	0.24/0.99; 0.86/0.41	32, 43	24, 14	7.3
(c) $\frac{1}{3}$ ML	1.47	0.19, 0.12	0.07, 0.07	73, 52	0.08/0.32; 0.24/0.11	0.38/0.92; 0.94/0.60	40, 37	18, 10	15.3
(d) $\frac{1}{3}$ ML	1.47	0.15, 0.19	0.01, 0.14	75, 70	0.04/0.38; 0.29/0.08	0.45/1.02; 0.89/0.46	40, 37	18, 14	12.1
(e) $\frac{1}{3}$ ML	1.41	0.25, 0.08	0.06, 0.07	70, 76	0.11/0.20; 0.58/0.08	0.78/0.81; 1.20/0.12	34, 23	33, 0	6.5
(f) $\frac{1}{6}$ ML	1.13	0.24	0.06	85	0.52/0.06	1.05/0.23	32	26	4.2
(g) $\frac{1}{6}$ ML	1.16	0.20	0.08	73	0.10/0.37	0.41/0.96	40	17	10.7
(h) $\frac{1}{6}$ ML	1.26	0.12	0.07	52	0.11/0.26	0.61/0.93	38	9	39.9
(i) $\frac{1}{6}$ ML	1.14	0.30	0.11	76	0.41/0.01	0.89/0.43	40	14	16.1
DFT [10]									
Homochiral	0.00[d]	0.40, 0.08		67, 49		0.96/0.48; 1.26/0.10	25, 17	35, 14	4.4
Heterochiral	0.13[d]	0.14, 0.20	0.01, 0.03	82, 62	0.05/0.29; 0.35/0.08	0.99/0.70; 1.09/0.43	36, 36	20, 9	13.1
Monomer		0.12				0.98/0.70	36	12	22.1

d(O–Cu) and d(N–Cu) refer to lateral distances from the nearest Cu atom paralled to the $[0\,0\,1]$ and $[1\bar{1}0]$ directions. The angles $\alpha_{O\text{–}O}$, $\alpha_{O\text{–}C\text{–}O}$, and $\beta_{C\text{–}N}$ are explained in Fig. 12. $I_{[0\,0\,1]}/I_{[1\bar{1}0]}$ is the intensity ratio between the π resonance with $\vec{E}\|[0\,0\,1]$ and $\|[1\bar{1}0]$.
[a] Expected ratio calculated from coordinates, except for NEXAFS.
[b] This work.
[c] Angle calculated from published coordinates.
[d] Relative adsorption energies.

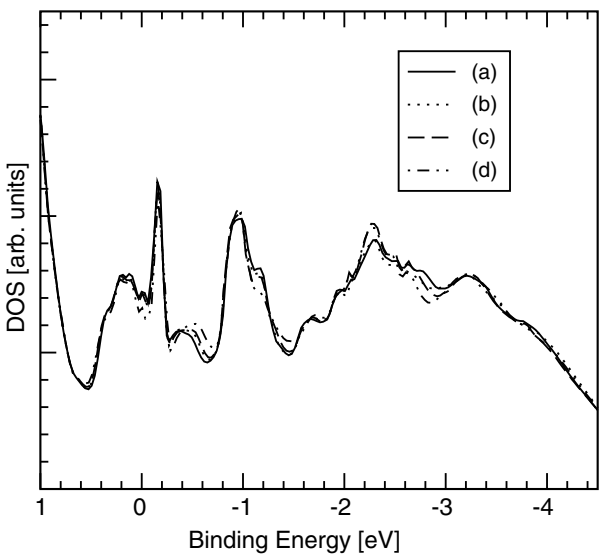

Fig. 2. Calculated DOS for the four enantiopure $p(3\times2)$ alanine overlayer geometries (a)–(d), shown in Fig. 1. Positive/negative binding energies correspond to occupied/unoccupied electronic states below/above the Fermi level.

the $p(3\times2)$ overlayer. The figure illustrates that the electronic structures of these geometries are very similar and largely independent of the local conformation. The calculated vacuum level was 4.43 eV in good agreement with the experimental workfunction value of 4.48 eV [28].

The NEXAFS spectra discussed in this paper are all excited from 1s orbitals. As a consequence of the dipole selection rule the destination orbitals (Ψ_{final}) must be of p-symmetry when starting from an s-orbital. The local density of states was projected onto atomic p-orbitals (p-LDOS) for carbon, nitrogen and oxygen to provide qualitative insight into the electronic symmetry and, hence, whether a transition is expected to be symmetry-allowed. The p-LDOS spectra for each atom are shown in the bottom parts of Figs. 6–8. They indicate which orbital energies would contribute to a NEXAFS spectrum below the vacuum level. To give further insight, the Kohn–Sham-orbitals corresponding to the peak in the p-LDOS were visualised (Fig. 11). Despite these orbitals not being the true wave functions, they are expected to be a good approximation and, hence, illustrate the essential spatial characteristics of the orbitals.

3. Experiment

The experiments were performed at beamline UE52-PGM of BESSY II in Berlin (Germany). The two-chamber ultra-high vacuum (UHV) end station is described elsewhere [29]. At the time of the experiments the base pressure was 3×10^{-10} mbar. XP spectra in the C 1s, N 1s, and O 1s regions were recorded using a Scienta 200 mm electron energy analyser with a pass energy of 40 eV and linearly polarised synchrotron radiation with a photon energy of 630 eV. The angle of incidence was close to the surface normal and the emission angle around 60° away from the surface normal. The binding energies (BE) were calibrated by measuring the Fermi edge with the same monochromator

and analyser parameters (photon energy, pass energy) after each change in the beamline settings.

The NEXAFS data shown here were recorded with the photon beam either at normal incidence or at angles of 35° or 70° with respect to the surface normal. The sample was mounted with its $[1\bar{1}0]$ crystallographic direction parallel to the manipulator axis, hence the angle of incidence was always in the plane perpendicular to this direction. The UE52 undulator at BESSY II allows the polarisation vector of the synchrotron radiation to be varied. For most of the experiments described here linear polarisation was used either horizontal or vertical to the plane of the storage ring. This led to orientations for the electrical field vector, $\vec{E}$, either parallel to the [0 0 1] or the $[1\bar{1}0]$ direction, respectively, i.e. perpendicular or parallel to the close packed rows of Cu atoms (cf. Fig. 1). A partial yield detector (PYD), positioned at grazing emission angle, was used for recording the secondary electron yield. The PYD retarding voltage was set to about 50 eV below the lowest photon energy in each spectrum, in order to avoid structures due to Cu 3s and 3p photoelectrons. The raw NEXAFS data were normalised with respect to the ring current, and divided by corresponding spectra of the clean sample, recorded under identical conditions [16,30]. The spectra shown here are the average of results from several independent experiments.

The Cu sample was prepared using standard procedures. These comprised electro-polishing, Ar-ion sputtering (typically 20 min at 1 μA/600 V) and oxygen treatment (5 min at 700 K in 5×10^{-7} mbar oxygen) in UHV followed by a final annealing step to 1000 K [31]. Surface cleanliness was checked by XPS; likely contaminants were found to be below the detection limit (<1%) in all cases.

Enantiopure *R* or *S*-alanine (99% from Aldrich) was adsorbed by evaporation from a custom-built evaporation source following closely the procedures established by Williams et al. [5,6]: a coverage in excess of the amount actually needed was deposited at room temperature followed by annealing to 360 K or 450 K in order to create the chiral $\begin{pmatrix} 2 & -2 \\ 5 & 3 \end{pmatrix}$ or the achiral pseudo-(3×2) overlayer structures, respectively. The latter structure is the main subject of this study. The long-range order of the adsorbate layer was checked by LEED prior to the XPS or NEXAFS experiments. The expected diffraction patterns were always observed, occasionally with somewhat broadened spots. All experimental data were recorded at room temperature if not specified otherwise.

4. Experimental results and their interpretation

4.1. XPS results

4.1.1. Alanine multilayers

For comparison with the chemisorbed alanine layers, the top spectra of Figs. 3–5 show C 1s, N 1s and O 1s XP spectra, respectively, of an about 50 Å thick layer of *S*-alanine (thickness estimated from the attenuation of the Cu 3d

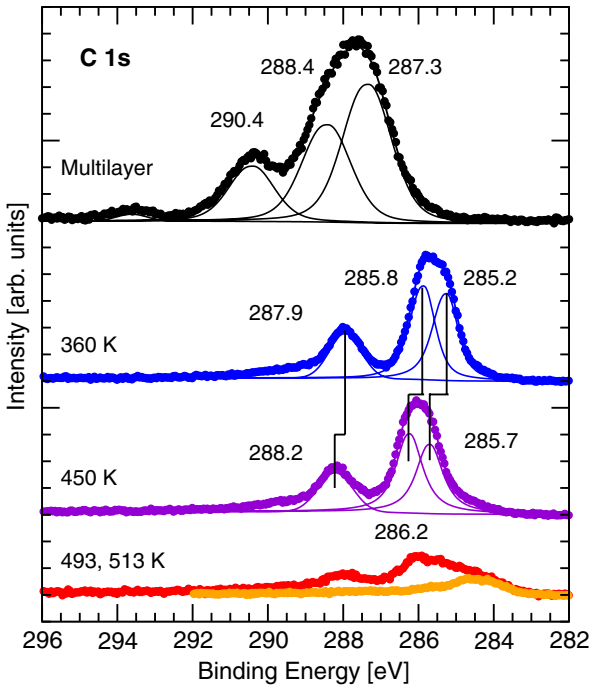

Fig. 3. C 1s XP spectra ($h\nu = 630$ eV, emission angle 60° from surface normal) of alanine on Cu{1 1 0}. Top spectrum: multilayer (*S*-alanine) adsorbed at 100 K; bottom spectra: *R*-alanine adsorbed at 300 K, annealing steps to 360 (chiral (2 −2; 5 3) overlayer), 450 (pseudo-(3×2) overlayer), 493, 513 K.

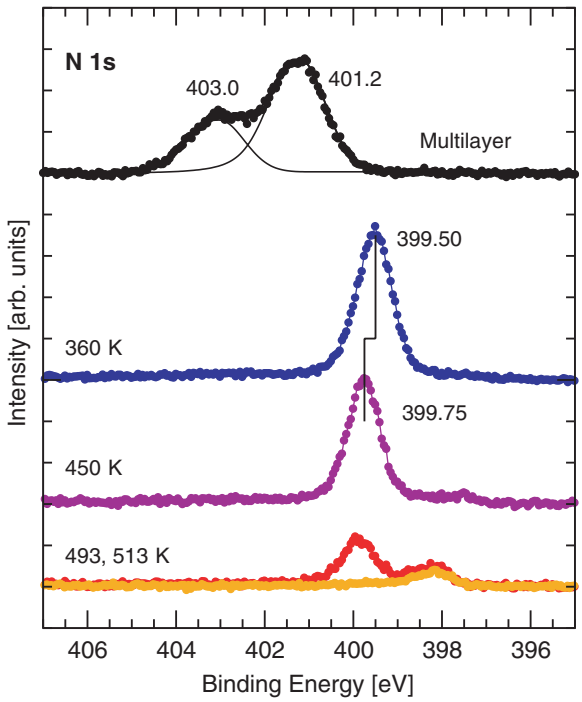

Fig. 4. N 1s XP spectra ($h\nu = 630$ eV, emission angle 60° from surface normal) of alanine on Cu{1 1 0}. Top spectrum: multilayer (*S*-alanine) adsorbed at 100 K; bottom spectra: *R*-alanine adsorbed at 300 K, annealing steps to 360 (chiral (2 −2; 5 3) overlayer), 450 (pseudo-(3×2) overlayer), 493, 513 K.

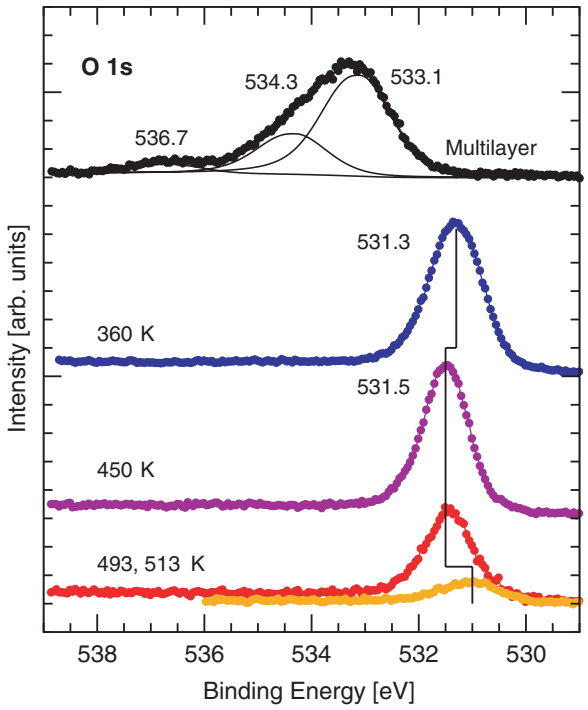

Fig. 5. O 1s XP spectra ($h\nu = 630$ eV, emission angle 60° from surface normal) of alanine on Cu{1 1 0}. Top spectrum: multilayer (*S*-alanine) adsorbed at 100 K; bottom spectra: *R*-alanine adsorbed at 300 K, annealing steps to 360 (chiral (2 −2; 5 3) overlayer), 450 (pseudo-(3 × 2) overlayer), 493, 513 K.

XPS signal) at 100 K. Unlike the gas phase XP spectrum published by Powis et al. [32], where the three carbon atoms of alanine lead to three well resolved C 1s peaks, only two peaks can be resolved in the spectrum of the multilayer (Fig. 3). The width of the dominating peak around BE 288 eV (FWHM 2.2 eV) is, however, comparable to the separation of the two peaks assigned to methyl (–CH_3) and the central (–$CH(NH_2)$–) carbon atoms in the gas phase spectrum. Therefore, we assign this peak to the overlap of the signals from these two atoms. The smaller peak at BE 290.4 eV is assigned to the carboxylate/carboxylic acid group (–COO^-/–COOH). Its energy separation from the centre of the other two peaks (2.6 eV) is significantly smaller than that in the gas phase spectra (3.5 eV). This is most likely a consequence of the fact that the molecules in the multilayer are predominantly in a zwitterionic state (CH_3–$CH(NH_3)^+$–COO^-) as is expected for solid alanine. Both the double peak in the N 1s multilayer spectrum (Fig. 4) and the large width of the O 1s peak (Fig. 5, FWHM 2.1 eV), which can be deconvoluted into two peaks, indicate that there are actually two different alanine species present in the multilayer. They may be a combination of neutral and zwitterionic species or simply surface and bulk species. XP spectra of thick glycine multilayers on Pt{1 1 1} [33] also show two N 1s peaks with a similar BE difference and asymmetric broadening in the O 1s signal, which have been assigned to the coexistence of a neutral and zwitterionic species. Noticeable satellite peaks are only observed in the C 1s and O 1s spectra at 293.6 and 536.7 eV, respectively. Therefore they are assigned to excitations related to the carboxylate group.

4.1.2. Chemisorbed alanine layers: coverage and temperature dependence

The other spectra in Figs. 3–5 were taken after *R*-alanine was adsorbed on Cu{1 1 0} at 300 K, followed by annealing to the indicated temperatures. The spectra for the *S*-enantiomer adsorbed under the same conditions were identical.

Annealing to 360 K leads to the formation of the ordered chiral overlayer structure described by the matrix $\begin{pmatrix} 2 & -2 \\ 5 & 3 \end{pmatrix}$. The long-range order, as observed in LEED, is improved significantly by the annealing step but the XP spectra are essentially the same as after adsorption at room temperature (not shown). With respect to the multilayer spectra, all peaks are shifted towards lower BE by an average of about 2 eV. The peaks are very similar in shape and BE to those published previously for the low and high coverage disordered phases [6]. In contrast to the multilayer, the N 1s and O 1s spectra now only show one narrow peak each, at BE 399.5 and 531.3 eV, indicating a single molecular species. In particular, the fact that only one O 1s peak is observed strongly indicates that both oxygen atoms are in an electronically similar environment. This implies that all chemisorbed molecules in this layer are deprotonated alaninates (–COO) with identical oxygen atoms rather than alanine (–COOH), for which a splitting of the O 1s signal would be expected. This finding is in agreement with spectra reported for acetate and glycinate on the same surface [17]. The observation of an asymmetric C–O stretch mode for this phase in RAIRS [6], however, indicates that the two oxygen atoms are in inequivalent positions with respect to the surface plane, which seems to contradict this interpretation; further experiments are planned to solve this puzzle. As for the multilayer, only two peaks are resolved in the C 1s spectrum. We assign the high BE peak at 288.0 eV to the carboxylate group. The lower BE feature centred at 285.6 eV has a higher peak area and a very asymmetric shape, which both indicate that it consists of the overlapping signals of the remaining two carbon atoms. A good fit to this feature can be achieved by two peaks with identical width at a separation of 0.61 eV. Assuming the same order as in the gas phase spectrum [32], the lower BE peak (285.24 eV) is assigned to the methyl and the higher BE peak (BE 285.85) to the central carbon atom.

For the pseudo-(3 × 2) layer, formed after annealing to 450 K, the N 1s and O 1s peaks are slightly narrower (FWHM 0.9 vs 1.0 eV and 1.0 vs 1.2 eV for N 1s and O 1s, respectively) than for the $\begin{pmatrix} 2 & -2 \\ 5 & 3 \end{pmatrix}$ structure, which we interpret as a sign of higher degree of homogeneity in this structure, as suggested by the comparison of structural models proposed for the two types of overlayers [6]. In addition, an upward shift in BE is observed by 0.2 eV for the O 1s and N 1s peaks and around 0.4 eV in the C 1s

peaks. The separation between the two C 1s peaks in the low BE feature (0.54 eV) is, however, almost the same as for the chiral overlayer. The integrated C 1s signal intensity is 10% lower than for the chiral overlayer. Since all XP spectra were recorded with the same photon energy of 630 eV the C 1s photoelectrons should be least affected by diffraction effects due to their high kinetic energy and, hence, provide a quantitative measure for the alanine coverage. The reduction in coverage is in agreement with a small desorption signal between 360 and 450 K.

The C 1s XP spectrum for the pseudo-(3×2) overlayer is in excellent agreement with the spectrum reported by Polcik et al. [8] for the same system under similar preparation conditions. Compared to the spectrum for glycine on Cu{1 1 0} reported by Hasselström et al. [17], the low BE peak is significantly broadened and more intense due to fact that alanine contains one more singly bonded carbon atom than glycine. The O 1s spectra of glycine and alanine are almost identical, indicating very similar O-surface bonds in both cases.

Annealing to 493 K leads to the decomposition and desorption of some alaninate, which is indicated by an overall decrease in the XPS signal intensities (about 50% for C 1s) and the appearance of new peaks around BE 284.4 and 398.3 eV in the C 1s and N 1s spectra, respectively. The peak position in the O 1s spectrum only changes after annealing to 513 K, indicating that the carboxylate group is thermally more stable than the rest of the molecule. This is in good agreement with earlier TPD experiments [6], which show that the main desorption peak of molecular fragments at around 520 K contains a large fraction of mass 44 (CO_2), and the dissociation mechanism proposed by Löfgren et al. [33] for glycine on Pt{1 1 1}, in which the first reaction step involves fission of the C–C bond.

4.2. NEXAFS results

4.2.1. Chemisorbed pseudo-(3×2) overlayer

C, N, and O K-edge NEXAFS spectra of the pseudo-(3×2) overlayer are shown in Figs. 6–8, respectively. The figures show spectra of *R*- and *S*-alanine recorded with the electric field vector $\vec{E}$ parallel to the $[1\bar{1}0]$ (lower spectra) and [0 0 1] (upper spectra) crystallographic directions, i.e. parallel and perpendicular to the close packed rows of Cu atoms, respectively (cf. Fig. 12). In all cases, the spectra of the two enantiomers are essentially identical. This indicates that the local adsorption geometries for the *R* and *S* enantiomers are related by the mirror planes of the substrate, parallel to the $(1\bar{1}0)$ and (0 0 1) crystallographic planes, in which $\vec{E}$ is oriented.

The O spectra (Fig. 8) are remarkably similar to the corresponding spectra for glycinate on Cu{1 1 0} [17], from which we conclude that the adsorption geometries of the carboxylate groups are very similar for both molecules. Besides the sharp π^* resonance at 533.1 eV, three additional features are observed. They have been assigned earlier to a multi-electron excitation (535.7 eV) and σ resonances due to C–C (539.7 eV) and C–O bonds (544 eV) [15–17].

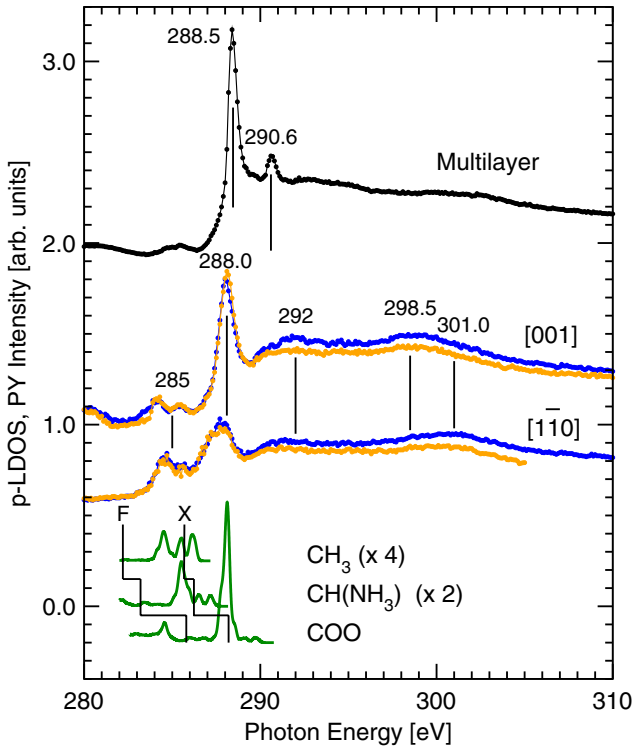

Fig. 6. Carbon K-edge NEXAFS spectra. Top spectrum: multilayer *S*-alanine adsorbed at 100 K, recorded with (+)-circularly polarised light in order to avoid polarisation effects; middle spectra: pseudo-(3×2) layers of *R*- and *S*-alanine (dark/light) with $\vec{E}\|[0\,0\,1]$ (upper spectra) and $\vec{E}\|[1\,\bar{1}\,0]$ (lower spectra); bottom: p-LDOS near the methyl (CH_3), central (C*), and carbolylate (COO) carbon atoms.

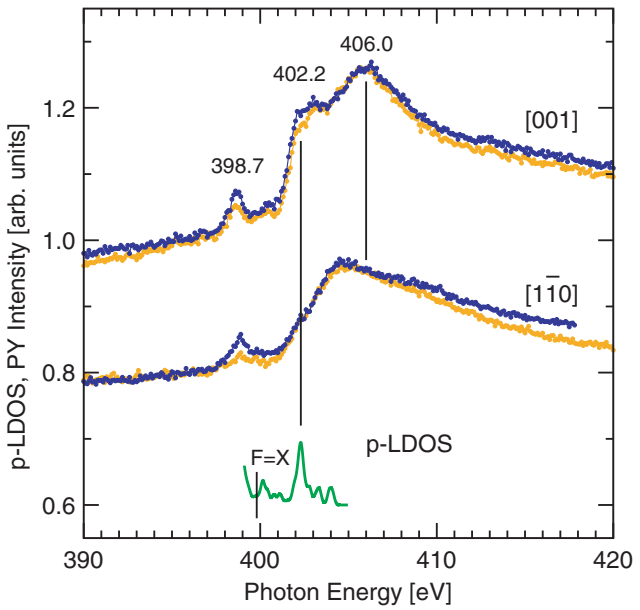

Fig. 7. Nitrogen K-edge NEXAFS spectra for pseudo-(3×2) layers of *R*- and *S*-alanine (dark/light) with $\vec{E}\|[0\,0\,1]$ (upper spectra) and $\vec{E}\|[1\,\bar{1}\,0]$ (lower spectra). Bottom: p-LDOS near the nitrogen atom.

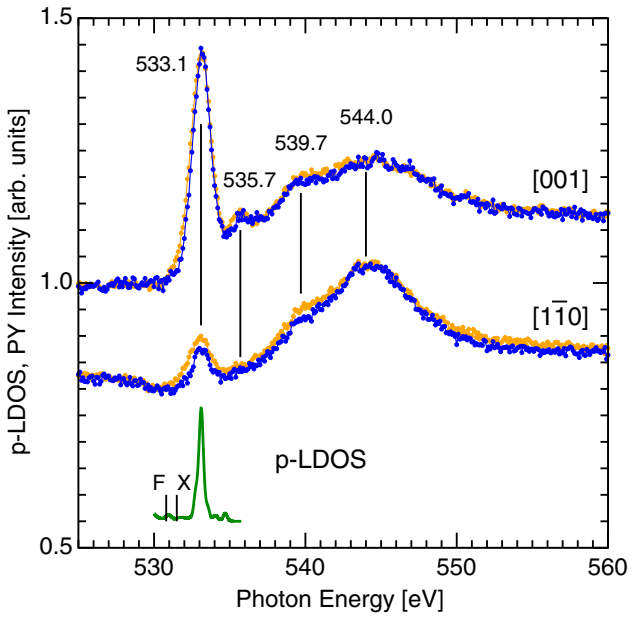

Fig. 8. Oxygen K-edge NEXAFS spectra for pseudo-(3 × 2) layers of *R*- and *S*-alanine (dark/light) with $\vec{E}\|[001]$ (upper spectra) and $\vec{E}\|[1\bar{1}0]$ (lower spectra). Bottom: p-LDOS near the oxygen atoms.

The N and C K-edge spectra show subtle differences with respect to those for glycine. In the C spectra for the chemisorbed layer (Fig. 6) features are observed around 285 eV with both polarisations. Similar features were predicted theoretically by Plashkevych et al. for the isolated molecule [34,35], mainly due to excitations from the methyl and central carbon atom into the π^* orbital. Such features do not appear in the experimental inner shell electron energy-loss gas-phase spectra published by Cooper et al. [36], however a broad feature at this energy is observed in our multilayer NEXAFS spectrum shown at the top of Fig. 6. Hasselström et al. [17] associated small features at 286 eV in their glycine spectra with carbon impurities at the surface. Impurities giving rise to features the size of those observed here should be detectable in XPS. However no such signal was found in the course of our experiments. For the same reason we can also exclude beam-induced decomposition of alanine as origin of this feature. The main π^* resonance peak for the chemisorbed layers is observed at 288.0 eV, slightly lower than in the multilayer spectrum (288.4 eV). The shape resonance around 292 eV is associated with C–N and C–C bonds; it is centered at higher photon energies than in the multilayer spectrum (290.6 eV), indicating that at least some of these bonds are contracted in the chemisorbed molecule. This σ(C–N)/σ(C–C) resonance is more intense with $\vec{E}$ parallel to [1 0 0] but does not disappear in the $[1\bar{1}0]$ spectrum, which indicates that some of the C–C or C–N bonds are significantly tilted with respect to both directions. In this respect our spectra differ from the glycine spectra in [17]. This is expected because of the additional methyl group in alanine makes it impossible for all C–C and C–N bonds to be aligned in the same direction as it is the case for glycine. The other two σ resonances at 298.5 and 301 eV are associated with the C–O bonds. They exhibit the same polarisation dependence as that observed for glycine [17].

In comparison to the C and O spectra, the N spectra (Fig. 7) are relatively structureless. The NEXAFS intensity increases right from the Fermi energy, indicated by the position of the XPS binding energy (399.8 eV) in agreement with the calculated projected local density of states, also shown in Fig. 7. The σ(C–N) shape resonance at 406 eV is only observed for the [1 0 0] polarisation, indicating that this bond is essentially perpendicular to the close packed Cu rows. The assignment of the small peak at 398.7 eV is unclear. It cannot be an artefact induced by the normalisation procedure since the clean surface signal shows no structure in this energy range. Small amounts of impurities or beam-induced damage are, however, possible reasons (note that this feature is approximately a factor 5 smaller than the 286 eV feature in the C spectra). Similar features have also been observed in connection with the formation of peptide bonds [36], which is another possibility that cannot be excluded at this small scale.

The polarisation dependence of the π^* resonance in the carbon and oxygen spectra clearly shows that the carboxylate group is aligned with its O–O axis closer to the $[1\bar{1}0]$ than the [0 0 1] direction. Assuming that the intensity of the resonance depends on the angle γ between $\vec{E}$ and a vector normal to the O–C–O triangle according to $I_{\mathrm{res}} \propto \cos^2\gamma$ [16], we can extract the in-plane tilt angle with respect to the close packed Cu rows ($[1\bar{1}0]$) from the spectra in Figs. 6 and 8. From the ratio $I_{[0\,0\,1]}/I_{[1\,\bar{1}\,0]}$ in the C (3.6) and O spectra (5.2) we obtain angles of 28° and 24°, respectively. The out-of-plane tilt angle of the O–C–O triangle can be determined in a similar way from spectra with a non-zero

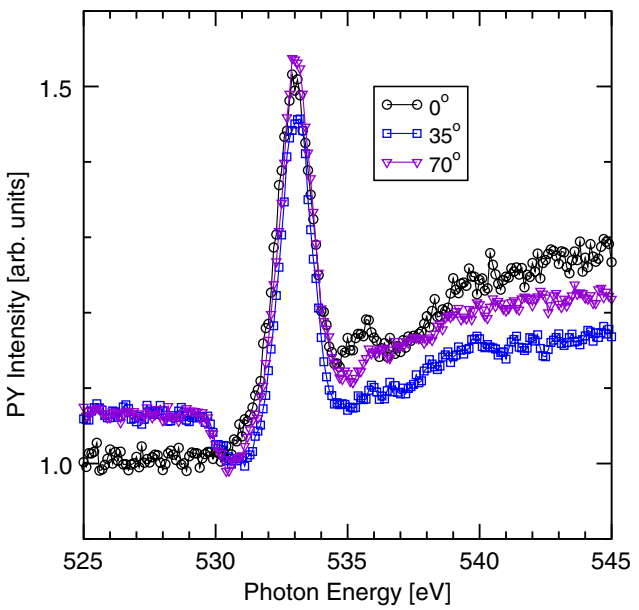

Fig. 9. Oxygen K-edge NEXAFS spectra from a pseudo-(3 × 2) layer of *S*-alanine for different angles of incidence. The angles indicated are those between the $\vec{E}$ vector and the surface plane (within the $(1\bar{1}0)$ plane).

perpendicular component of $\vec{E}$. As described in the experimental section, rotating the sample causes $\vec{E}$ to rotate within the $(1\,\bar{1}\,0)$ crystallographic plane. In our experiments, rotation by 35° and 70° did, however, not change the intensity of the π^* resonance by more than 10%, as shown in Fig. 9. This behaviour is compatible with a tilt angle of around 45° and equal numbers of molecules tilted in opposite directions within the $(1\,\bar{1}\,0)$ plane. Only in this case the relative phase shift of 90° in the angular dependencies of the π^* resonances from the two different types of carboxylate groups compensate each other and add up to an angle-independent intensity. Tilting in opposite directions is expected because of the C_2 symmetry of both the Cu{1 1 0} substrate and the (3×2) overlayer lattice. (3×2) domains rotated by 180° should, therefore, be energetically degenerate and exist in equal numbers.

4.2.2. Chiral (2 −2; 5 3) overlayer

The N and O NEXAFS spectra for the chiral $\begin{pmatrix} 2 & -2 \\ 5 & 3 \end{pmatrix}$ phases of both enantiomers (not shown) are identical to the spectra of the pseudo-(3×2) overlayers, implying that the local adsorption geometries, in terms of alignment of the two oxygens along the $[1\,\bar{1}\,0]$ direction and the out-of-plane tilt, are very similar in these two phases. We note that the RAIRS data for this phase suggests geometrically inequivalent oxygens, i.e. the O–O vector is tilted with respect to the surface plane. Our NEXAFS data do not allow such a tilt to be probed, therefore further experiments applying crystallographic techniques are needed to solve the puzzle why the oxygens appear electronically equivalent in the XPS data (Fig. 5) but geometrically inequivalent in the RAIRS data. Finally, subtle differences are observed in the carbon spectra, shown in Fig. 10, mainly with respect to the polarisation dependence of the σ(C–O) resonances at 298.5 and 301 eV. Unlike in the pseudo-(3×2) phase, these resonances do not show a clear polarisation dependence in the chiral phase. Since the polarisation dependence of the π^* resonance is unchanged, this cannot be due to a major reorientation of the carboxylate group. A more likely explanation is that the molecules are more distorted in the slightly denser chiral phase, which would affect the symmetry and, hence, the polarisation dependence of these excitations.

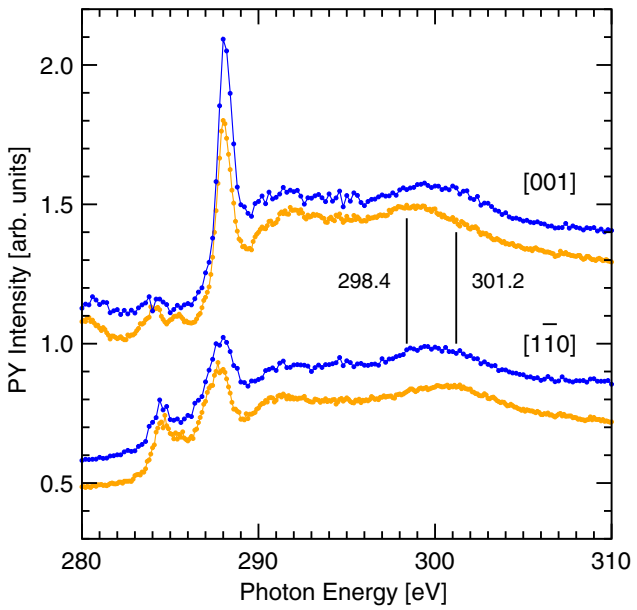

Fig. 10. Carbon K-edge NEXAFS spectra for *R*-alanine in the pseudo-(3×2) (light) and the chiral (2 −2; 5 3) phase (dark). Upper spectra: $\vec{E}\|[0\,0\,1]$; lower spectra: $\vec{E}\|[1\,\bar{1}\,0]$.

4.3. Electronic structure calculations

Fig. 2 illustrates that the calculated DOS for all four local conformations of the $p(3\times2)$ phase of alanine on Cu{1 1 0} are almost identical. The local conformation has very little bearing on the electronic structure, therefore, further analysis was carried out on only one of these structures, (c), shown in Fig. 1. Structure (c) was chosen mainly because it consists of both linear and kinked molecules, which allows the sensitivity of the electronic structure to the molecular geometry to be probed with a minimum computational effort.

From the p-LDOS curves plotted at the bottom of Figs. 6–8 it can be clearly seen that the largest p-character orbitals for C, N and O lie at approximately 2.3 eV above the Fermi level. Their spatial distribution is depicted in Fig. 11. The figure shows that the shape of the orbitals contributing most to the NEXAFS signal is essentially the same for both molecular configurations. The shapes of the p-LDOS curves are in good agreement with the prominent experimental peaks observed for C and O, when the energy scales are shifted accordingly. These shifts have to be applied for each atom separately. In particular, for the three carbon atoms, Fermi energy offsets of 282.2 (methyl), 283.3 (central), and 285.8 eV (carboxylate) had to be added in order to align the peaks with the relevant experimental features. We are using the same order of shifts here as it was found for the XPS peaks. The position of the Fermi energy is indicated by a vertical line (marked 'F') in each p-LDOS spectrum; also indicated are the corresponding XPS energies ('X'). For perfect screening, as in the case of a metal, the XPS energy would mark the 'Fermi edge' in the NEXAFS spectrum, i.e. the onset of the NEXAFS signal related to this particular atom [37]. The fact that the excitations from the methyl and central carbon atoms appear at significantly lower photon energies, up to 1.3 eV (cf. Fig. 6), implies, therefore, that these core holes are incompletely screened due to their large distance from the metal surface. The distance between the calculated Fermi energy and the XPS peak energy is due to a combination of a true shift of the π state with respect to the Fermi energy, as a result of the 1s ionisation (the p-LDOS is calculated for a non-ionised molecule), and the lack of screening discussed above. As expected, the carboxylate carbon has the highest contribution of the three chemically distinct carbon atoms to the p-LDOS in the relevant energy range.

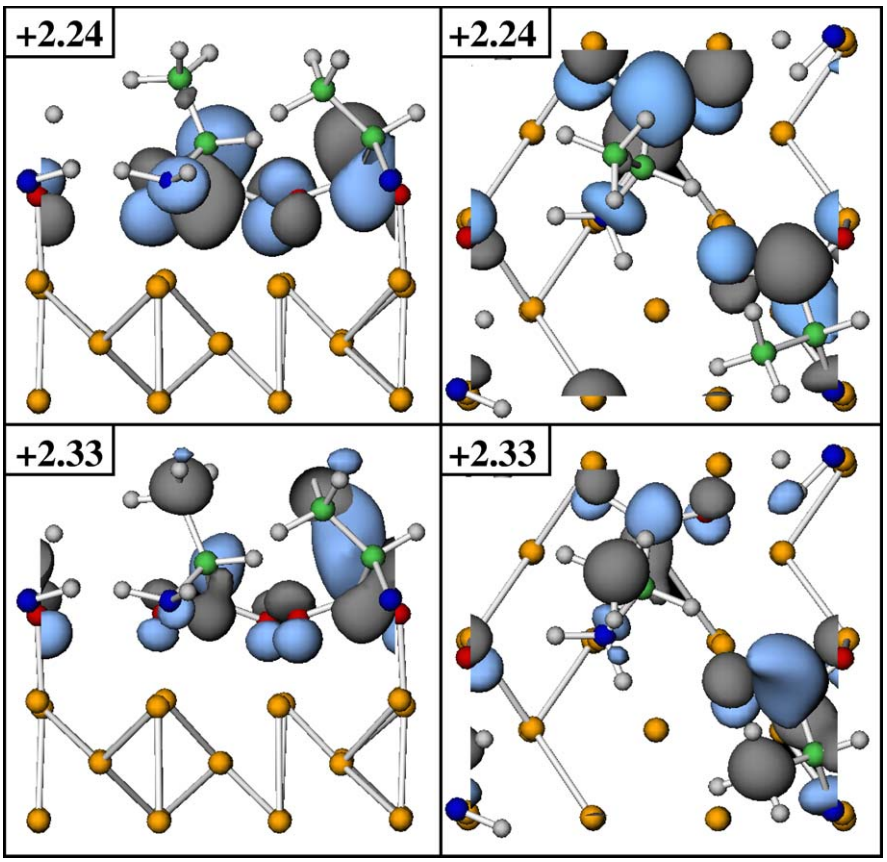

Fig. 11. Calculated Kohn–Sham orbitals of geometry (c) extracted from the Γ-point for the unoccupied states 2.24 and 2.33 eV above the Fermi level. Left: side view; right: top view; C green; H white; N blue; O red; Cu orange; iso-surfaces show the Kohn–Sham orbital, parity: + blue; − grey.

Its peak is more than twenty times as high as the contribution of the other carbon atoms.

The differences between the Fermi energy in the shifted p-LDOS spectra and the XPS energies are much smaller for N (≈0) and O (≈1 eV) since they are closer to the metal surface and, hence, more effectively screened. The alignment of the nitrogen p-LDOS is not as straight forward as that for C and O. Correlating the shoulder at 402 eV with the p-LDOS peak associated with the π state explains its polarisation dependence; it is the same as the π-resonance in the C and O spectra. Consequently, the peak at 404.5 eV in the $[1\,\bar{1}\,0]$ spectrum is assigned to the actual nitrogen K-edge.

5. Discussion and conclusions

The application of dipole selection rules to NEXAFS can be very useful in the determination of certain structural aspects of larger molecules. This is particularly helpful in the context of chiral adsorption systems which are too complex to be completely analysed by diffraction methods. Here we summarise our NEXAFS results for the pseudo-(3×2) phase and show that they are quite complementary to the earlier experimental results from PhD by Sayago et al. [9], who were able to locate the O and N atoms forming the molecular footprint on the surface, but not the positions of the carbon atoms forming the backbone of the molecule.

The structural parameters determined experimentally in this study, i.e. the tilt angles of the carboxylate group with respect to the surface plane (≈45°) and the $[1\,\bar{1}\,0]$ direction (≈26°) as well as the angle between the C–N bond and $[1\,\bar{1}\,0]$ (≈90°), are compatible with the earlier findings that the molecules assume a tridentate adsorption geometry with surface bonds through the two oxygen atoms and the nitrogen atom. In order to assume this geometry, the O–C–O plane must be tilted with respect to the surface plane. The previous PhD [9] and DFT [10] studies both agree that the O–O axis is tilted with respect to the close packed rows of Cu atoms along the $[1\,\bar{1}\,0]$ direction. This allows the C–N bond to be more or less perpendicular to that direction. The experimentally determined orientation of the C–N bond in particular is not compatible with all five geometry models (a)–(e) that lead to similar heats of adsorption in our DFT calculations. Their parameters are listed in Table 1, together with the experimentally determined parameters and those from the earlier DFT study [10]. It is difficult to estimate the error bar associated with the C–N bond angle, i.e. the degree to which the σ(C–N) shape resonance at 406 eV is absent in the $[1\,\bar{1}\,0]$ NEXAFS spectrum of Fig. 7. Also, Nyberg et al. [19] pointed out recently that the relative peak intensities in the nitrogen NEXAFS

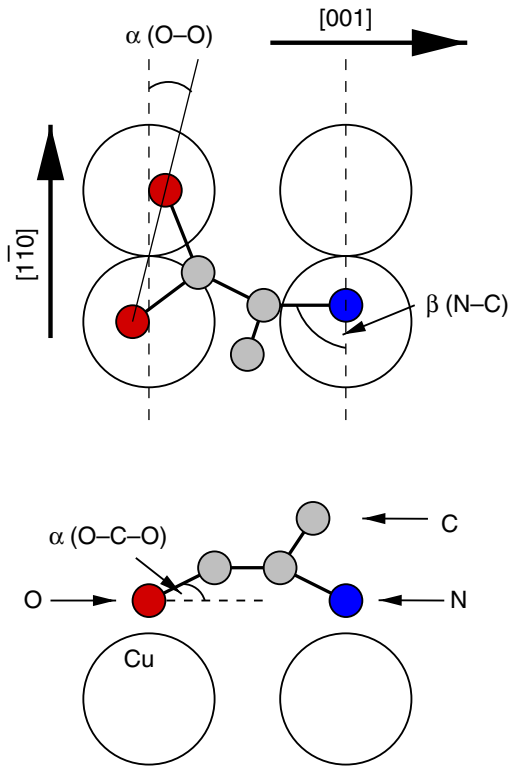

Fig. 12. Schematic drawing of the alanine adsorption complex on Cu{1 1 0} defining the tilt angles determined by NEXAFS. Top: top view; bottom: side view, cut along the [0 0 1] direction.

spectrum for glycine depend on the degree of hydrogen bonding between neighbouring amino acids. However, if one of the C–N bonds had an angle of $\beta = 52°$ with respect to the $[1\,\bar{1}\,0]$ direction of the Cu atom rows, as in geometries (a) and (c), this should lead to a σ(C–N) intensity in the $[1\,\bar{1}\,0]$ spectrum of around 30% of that in the [0 0 1] spectrum, which is clearly outside the error bar of the experiment. The other three geometries, (b), (d) and (e), lead to σ(C–N) intensity ratios of less than 10%, which is within the experimental error. With respect to the in-plane and out-of-plane tilt angles of the O–C–O group only (b) and (d) agree well with the experimental data. Both angles are within 13° of the experimental values whereas one out-of-plane and one in-plane angle in geometry (e) are more than 20° off. Since we always assumed unperturbed molecular orbitals in our angle determination from the NEXAFS spectra, distortions due to the interaction with the surface will add to the experimental error. Another contribution to the experimental error is, of course, the fact that the data analysis assumes identical angles for both types of molecules, which is not the case for the theoretically predicted structures. The deviation of 13° appears, therefore, acceptable. Taking into account all experimental results, including those from PhD, and the expected intensity ratios of the π resonance, $I_{[0\,0\,1]}/I_{[1\,\bar{1}\,0]}$, for the DFT models (all listed in Table 1) we find a better overall agreement for geometry (b), but (d) cannot be excluded. The fact that the two conformations lead to very similar heats of adsorption and the shallow nature of the potential energy surface make it not implausible that they could coexist on the surface. A closer examination of the two geometries reveals that the transition from one to the other is essentially a torsion of the molecular backbone. Vibrational modes associated with this motion have low frequencies and can probably be excited at room temperature. The fact that one of the structures, (b), which agree best with the experimental results is not among those most favoured by the calculated heats of adsorption is not a strong argument against it. One must take into account that the experimentally observed 'pseudo-(3×2)' domain structure has a long-range periodicity different from the perfect $p(3\times2)$ overlayer that was assumed in both theoretical studies. Given the small energy differences between all models studied theoretically, small differences in the local geometries near the domain boundaries can easily tip the balance in favour of a structure, which is less favoured in the perfect overlayer. Future work will have to focus on the interplay between the local adsorption geometry and its influence on the intermolecular bonding which determines the long-range order of these layers.

The experimental results also agree reasonably well with the 'heterochiral' geometry from the DFT study by Rankin and Sholl [10]. This is very similar to our geometry (d) and is energetically favoured with respect to their alternative 'homochiral' structure, which is similar, but not identical, to our geometry (e). At this point it is important to note again that the footprint geometry does not define the adsorbate conformation completely. With both 'heterochiral' and 'homochiral' footprints different stable combinations of 'linear' and 'kinked' backbone arrangements are found in our DFT study. The steric requirement that the methyl group needs to be directed away from the surface, the essentially tetrahedral coordination of the central carbon atom and the constraints arising from the three point binding motif, however, only allow kinking the molecule in one direction. Among other implications, this leads to important structural and energetic differences regarding the backbone arrangements between enantiopure and racemic layers of alanine. Such differences have recently been found theoretically by Rankin and Sholl [10,38] and in our own studies, but it is not clear from these studies whether an equal mixture of *R* and *S*-alanine on Cu{1 1 0} would form a racemic adlayer or separate into enantiopure islands, as the theoretically predicted adsorption energies per molecule are very similar in both cases. An experimental study of such layers might be able solve this problem and would be very helpful for the understanding of lateral interactions and steric constrains in alanine adlayers in general.

6. Summary

The adsorption of alanine on Cu{1 1 0} was studied by NEXAFS, XPS and DFT. Large chemical shifts in the C 1s, N 1s, and O 1s XP spectra were found between the

alanine multilayer and the chiral $\begin{pmatrix} 2 & -2 \\ 5 & 3 \end{pmatrix}$ and achiral pseudo-(3×2) chemisorbed alaninate layers. The similarities between the spectra of the two chemisorbed overlayers suggest that the molecules are in similar environments in terms of alignment of the two oxygen atoms with respect to the $[1\,\bar{1}\,0]$ direction and the out-of-of plane tilt of the carboxylate group. Five possible adsorption geometries for the $p(3\times2)$ overlayer were identified by DFT, which all lead to similar heats of adsorption between 1.40 and 1.47 eV/molecule. From C, N, and O K-shell NEXAFS spectra for different polarisations with respect to the main surface directions the tilt angles of the O–C–O carboxylate group ($\approx$26° in plane with respect to $[1\,\bar{1}\,0]$ and $\approx$45° out of plane) and the C–N bond angle with respect to $[1\,\bar{1}\,0]$ could be determined. Using this information three of the DFT structures can be eliminated. Due to the small energy difference between the remaining two structures it is not unlikely that these coexist on the surface at room temperature.

Acknowledgements

This study was supported by EPSRC, by the European Community Research Infrastructure Action under the FP6 "Structuring the European Research Area" Programme (through the Integrated Infrastructure Initiative "Integrating Activity on Synchrotron and Free Electron Laser Science – Contract R II 3-CT-2004-506008)", and by "Verein der Freunde und Förderer von BESSY". One of us (S.J.J) thanks The Royal Society for a University Research Fellowship. We also thank the BESSY staff for their help during the beamtime, in particular T. Schmidt and D. Batchelor, Z. Liu for his help with the preparation of Figs. 2 and 11, and R.B. Rankin and D.S. Sholl for sending us the full details of their DFT results.

References

[1] S.M. Barlow, R. Raval, Surf. Sci. Rep. 50 (2003) 201.
[2] F. Rosei, M. Schunack, Y. Naitoh, P. Jiang, A. Gourdon, E. Lægsgaard, I. Stensgaard, C. Joachim, F. Besenbacher, Prog. Surf. Sci. 71 (2003) 95.
[3] V. Humblot, S.M. Barlow, R. Raval, Prog. Surf. Sci. 76 (2004) 1.
[4] G. Jones, S.J. Jenkins, D.A. King, submitted for publication.
[5] J. Williams, S. Haq, R. Raval, Surf. Sci. 368 (1996) 303.
[6] S.M. Barlow, S. Louafi, D. Le Roux, J. Williams, C. Muryn, S. Haq, R. Raval, Surf. Sci. 590 (2005) 243.
[7] S.M. Barlow, S. Louafi, D. Le Roux, J. Williams, C. Muryn, S. Haq, R. Raval, Langmuir 20 (2004) 7171.
[8] M. Polcik, F. Allegretti, D.I. Sayago, G. Nisbet, C.L.A. Lamont, D.P. Woodruff, Phys. Rev. Lett. 92 (2004) 236103.
[9] D.I. Sayago, M. Polcik, G. Nisbet, C.L.A. Lamont, D.P. Woodruff, Surf. Sci. 590 (2005) 76.
[10] R.B. Rankin, D.S. Sholl, Surf. Sci. Lett. 574 (2005) L1.
[11] N.A. Booth, D.P. Woodruff, O. Schaff, T. Gießel, R. Lindsay, P. Baumgärtel, A.M. Bradshaw, Surf. Sci. 397 (1998) 258.
[12] R.B. Rankin, D.S. Sholl, Surf. Sci. 548 (2004) 301.
[13] N.V. Richardson, A.M. Bradshaw, Photoelectron spectroscopy – Theory, Techniques and Applications, vol. 4, Academic Press, New York, 1981.
[14] H.-P. Steinrück, J. Phys. Condens. Matter 8 (1996) 6465.
[15] J. Somers, A.W. Robinson, T. Lindner, D. Ricken, A.M. Bradshaw, Phys. Rev. B 40 (1989) 2053.
[16] J. Stöhr, NEXAFS Spectroscopy, second ed., Springer Series in Surface Sciences, Springer, Berlin, 1996.
[17] J. Hasselström, O. Karis, M. Weinelt, N. Wassdahl, A. Nilsson, M. Nyberg, L.G.M. Petterson, M.G. Samant, J. Stöhr, Surf. Sci. 407 (1998) 221.
[18] J. Nyberg, M. Hasselström, O. Karis, N. Wassdahl, M. Weinelt, A. Nilsson, L.G.M. Petterson, J. Chem. Phys. 112 (2000) 5420.
[19] M. Nyberg, M. Odelius, A. Nilsson, L.G.M. Petterson, J. Chem. Phys. 119 (2003) 12577.
[20] W. Kohn, L. Sham, Phys. Rev. 140 (1965) A1133.
[21] M.C. Payne, M.P. Teter, D.C. Allan, T.A. Arias, J.D. Joannopoulos, Rev. Mod. Phys. 64 (1992) 1045.
[22] D. Vanderbilt, Phys. Rev. B 41 (1990) 7892.
[23] J.P. Perdew, J.A. Chevary, S.H. Vosko, K.A. Jackson, M.R. Pederson, D.J. Singh, C. Fiolhais, Phys. Rev. B 46 (1992) 6671.
[24] H.J. Monkhorst, J.D. Pack, Phys. Rev. B 13 (1976) 5188.
[25] Q. Chen, D.J. Frankel, N.V. Richardson, Surf. Sci. 497 (2002) 37.
[26] R.L. Toomes, J.-H. Kang, D.P. Woodruff, M. Polcik, M. Kittel, J.-T. Hoeft, Surf. Sci. 522 (2003) L9.
[27] A. Rassat, P.W. Fowler, Hel. Chim. Acta 86 (2003) 1728.
[28] D.R. Lide, H.P.R. Frederikse, Handbook of Chemistry and Physics, 76th ed., CRC Press, Boca Raton, 1995.
[29] R. Wichtendahl, Dissertation, Freie Universität Berlin, 1999.
[30] A. Schöll, Y. Zou, T. Schmidt, R. Fink, E. Umbach, J. Electron, Spectrosc. Relat. Phenom. 129 (2003) 1.
[31] C. Ammon, A. Bayer, H.P. Steinrück, G. Held, Chem. Phys. Lett. 377 (2003) 163.
[32] I. Powis, E.E. Rennie, U. Hergenhahn, O. Kugeler, R. Bussy-Socrate, J. Phys. Chem. A 107 (2003) 25.
[33] P. Löfgren, A. Krozer, J. Lausmaa, B. Kasemo, Surf. Sci. 370 (1997) 277.
[34] O. Plashkevych, V. Carravetta, O. Vahtras, H. Ågren, Chem. Phys. 232 (1998) 49.
[35] L. Yang, O. Plashkevych, O. Vahtras, V. Carravetta, H. Ågren, J. Synchrotron Radiat. 6 (1999) 708.
[36] G. Cooper, M. Gordon, D. Tulumello, C. Turci, K. Kasnatcheev, A.P. Hitchcock, J. Electron Spectrsc. Relat. Phenom. 137–140 (2004) 795.
[37] A. Nilsson, O. Björneholm, E.O.F. Zdansky, H. Tillborg, N. Mårtensson, J.N. Andersen, R. Nyholm, Chem. Phys. Lett. 197 (1992) 12.
[38] R.B. Rankin, D.S. Sholl, J. Chem. Phys. B 109 (2005) 16764.